

V₂O₅ xerogel electrodes with much enhanced lithium-ion intercalation properties with N₂ annealing

Dawei Liu,^a Yanyi Liu,^a Betzaida Batalla Garcia,^a Qifeng Zhang,^a Anqiang Pan,^{ab} Yoon-Ha Jeong^c and Guozhong Cao^{*a}

Received 17th July 2009, Accepted 17th September 2009

First published as an Advance Article on the web 7th October 2009

DOI: 10.1039/b914436f

V₂O₅ xerogel films were fabricated by casting V₂O₅ sols onto FTO glass substrates and annealing at 300 °C for 3 hours in nitrogen and air. The films annealed in nitrogen and air possessed different grain size and crystallinity. Optical absorption measurements and electrochemical impedance analyses revealed a reduced optical bandgap and enhanced electrical conductivity of N₂ annealed V₂O₅ film. Lithium ion intercalation measurements showed that at a charge/discharge current density of 600 mA g⁻¹, the N₂ annealed sample possessed noticeably better lithium ion storage capability. In contrast to the air annealed sample, which started with a discharge capacity of 152 mAh g⁻¹ but after 50 cycles the capacity had decreased to a low value of only 44 mAh g⁻¹, the N₂ annealed sample started with a low value of 68 mAh g⁻¹ but the capacity increased sharply to a high value of 158 mAh g⁻¹ at the 24th cycle, followed by little capacity degradation in later cycles and after 50 cycles, the discharge capacity was still as high as 148 mAh g⁻¹. Much improved lithium ion intercalation capacity and cyclic stability could be attributed to surface defects V⁴⁺ and/or V³⁺ and associated oxygen vacancies introduced by N₂ annealing as well as much less crystallized vanadium oxide.

1. Introduction

V₂O₅, as an active lithium ion intercalation host, has been intensively studied as the positive electrode material for lithium ion batteries for the past decades^{1–3} and has recently been commercialized by Panasonic.⁴ V₂O₅ electrodes fabricated by various methods like sputtering,⁵ thermal evaporation,⁶ electro-phoretic deposition⁷ and sol–gel casting⁸ were all studied for their lithium ion intercalation capabilities. Chemical composition, crystal structure and crystallinity, and micro- and nanostructures were all found to play critical roles in determining lithium ion intercalation capacities and cyclic stabilities.^{9,10} However, even with optimized micro, and nanostructures and crystallinity, the practical application of vanadium oxides in lithium ion batteries was still limited by the relatively poor cyclic stability,¹¹ though this is a general concern for most lithium ion intercalation electrodes and researchers have been actively searching for effective methods to solve this problem. Surface coating has shown to be a viable method to improve the intercalation cyclic stability. For example, a thin layer of carbon or inert oxides could prevent the active material (electrode) from dissolution in the electrolyte while at the same time improving the electrode/electrolyte interfacial charge transfer process.^{12–14} This surface coating has already been successfully used on commercialized cathode materials, such as LiCoO₂ with well improved cyclic stability.^{15,16} However, the established coating techniques were often

complicated and the uniformity of the coating was another challenge.¹⁷ In our earlier work, it was found that annealing TiO₂ nanotube arrays fabricated by means of anodization in reducing gas CO resulted in much improved lithium ion intercalation properties.¹⁸ After annealing in CO, the surface layer of TiO₂ nanotubes contained both carbide species and oxygen vacancies,¹⁹ which were found to help enhance the lithium ion intercalation capabilities of the host electrode owing to the possible role of such surface point defects as nucleation centers for phase transformation during the lithium ion insertion and extraction processes. Such defects may also reduce the stress and the electrostatic repulsion between adjacent oxygen layers.²⁰ In addition, this thin surface layer could play a similar role as protecting coating on active electrode. For example, LiFePO₄ with a less crystallized thin surface layer which was created by treating in inert Ar gas was found to exhibit better cyclic stability.²¹ Compared with other surface treatment methods like ion sputtering,²² electron beam exposure²³ and low energy ultraviolet photon illumination,²⁴ thermal annealing in reducing or inert gas atmosphere does not require a delicate facility and has the advantages of easy control of experimental conditions. For vanadium pentoxide thin film electrode, it was reported that annealing in an ultrahigh vacuum was a good way to introduce V⁴⁺ and V³⁺ ions.²⁵ The conductivity of the film was proven to be enhanced due to the presence of lower valence vanadium ions and associated oxygen vacancies. In this study, we compared sol–gel derived V₂O₅ films, annealed under respective nitrogen and air flows, and compared their crystal structures, crystallinity, and electrochemical properties. It was found that sol–gel derived V₂O₅ films can possess significantly different microstructure and crystallinity, lithium ion intercalation properties and cyclic stability when annealed under different conditions. The

^aDepartment of Materials Science and Engineering, University of Washington, Seattle, USA. E-mail: gzc@u.washington.edu

^bDepartment of Materials Science and Engineering, Central South University, Changsha, P. R. China

^cNational Center for Nanomaterials Technology (NCNT), Pohang University of Science and Technology, Pohang, South Korea

dependence of lithium intercalation properties of V_2O_5 films on the annealing has been discussed.

2. Experimental

A diluted sol of $V_2O_5 \cdot nH_2O$ was prepared using a method reported by Fontenot *et al.*²⁶ In brief: 0.136 g V_2O_5 powder was dissolved in 2 ml de-ionized water and 0.603 ml 30% H_2O_2 solution. The suspension was stirred until V_2O_5 powder totally dissolved, resulting in a clear and dark red solution. The solution was then sonicated to get a yellow-brown gel which was dispersed into de-ionized water in a molar concentration of 0.005 M with primary vanadium species in the colloidal dispersion nanoparticles of hydrated vanadium oxide. $V_2O_5 \cdot nH_2O$ films were then prepared by spreading 50 μ l of $V_2O_5 \cdot nH_2O$ sol onto fluorine-doped tin oxide (FTO) glass substrates. After drying under ambient conditions for 24 h, the films were then annealed at 300 °C for 3 h in respective dry N_2 and air flow (300 °C was the necessary annealing temperature to induce phase transition in vanadium oxide based on the literature⁸ and the annealing time of 3 h appeared to be good enough to obtain stabilized crystallinity. In addition, they were good enough to create low valence V ions on V_2O_5 in N_2 annealing). Vanadium oxide xerogels were thus obtained by dehydration of vanadium oxide gels. After nitrogen annealing, the originally yellow-brown film turned dark green while the color of the film annealed in air did not change much.

Scanning electron microscopy (SEM, Philips, JEOL JSM7000) and X-ray diffraction (XRD, Philips 1820 X-ray diffractometer) were carried out to characterize the morphology and crystallization state of annealed films. Optical absorption spectra of the V_2O_5 films annealed in different gas atmospheres were measured in the wavelength range 300–800 nm using a fiber optic spectrometer (Ocean Optics, Inc.). An electrochemical impedance spectroscopy study was carried out using a Salon 1260 impedance/gain-phase analyzer with platinum foil as a counter electrode and 1 M $LiClO_4$ in propylene carbonate as the electrolyte. The range of the frequency was from 100 kHz to 0.05 Hz. Lithium ion intercalation properties of V_2O_5 films were investigated using a standard three-electrode system, with 1 M $LiClO_4$ in propylene carbonate as the electrolyte, a Pt mesh as the counter electrode, and $Ag/AgCl$ as the reference electrode. Cyclic voltammetric (CV) tests were conducted between 0.6 V and -1.4 V (~ 3.7 V and 1.7 V vs. Li^+/Li) with a scan rate of 10 $mV s^{-1}$; chronopotentiometric (CP) tests were carried out in the voltage range from 0.6 V to -1.4 V with current density of 200 $mA g^{-1}$, 600 $mA g^{-1}$, 1 $A g^{-1}$, 2 $A g^{-1}$ and 5 $A g^{-1}$. Both the CVs and CPs were done by using an electrochemical analyzer (CH Instruments, Model 605B).

3. Results and discussion

The sol-gel derived V_2O_5 films were homogeneous with a smooth and featureless surface morphology; no detectable cracks or pinholes were observed and the film thickness was $\sim 1 \mu m$, similar to the results reported earlier.⁸ The porosity of the as fabricated film at room temperature was estimated to be about 54% through density measurement and calculation. No morphology difference was found in the as fabricated V_2O_5 films and the films annealed in air and nitrogen as revealed by means of SEM images

Table 1 Interlayer spacing and grain size of V_2O_5 films annealed in air and nitrogen at 300 °C for 3 h

| Film | Interlayer spacing (\AA) | Grain size (nm) |
|--------------|-------------------------------------|-----------------|
| 300 °C Air | 11.0 | 14.3 |
| 300 °C N_2 | 11.5 | 5.1 |

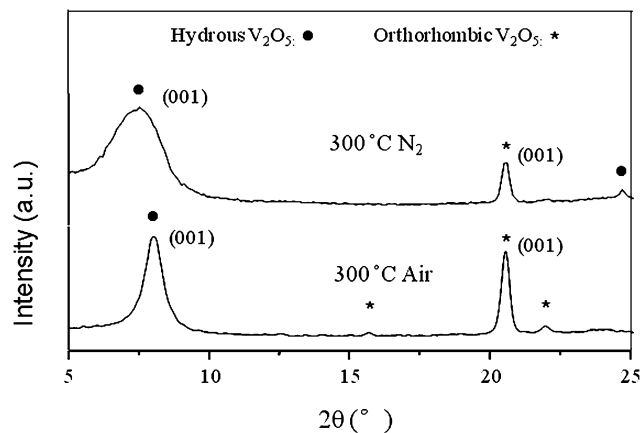


Fig. 1 X-Ray diffraction patterns of V_2O_5 xerogel films annealed in air and nitrogen at 300 °C after 3 h, showing the coexistence of both hydrus and orthorhombic vanadium oxide.

(not shown here). However, the annealing did result in an appreciable change in crystal structure or phase transition and grain growth. Fig. 1 compares the XRD patterns of V_2O_5 films annealed in respective air and nitrogen at 300 °C for 3 h. Hydrus V_2O_5 and orthorhombic V_2O_5 were found to coexist in both samples, indicating there was a partial phase transition. A closer look reveals that the diffraction peaks from the film annealed in nitrogen possessed much broader full width at half-maximum than that in air annealed film with a position shift of (001) peak of hydrus V_2O_5 towards lower angle. The interlayer distance and grain size have been calculated from the diffraction angle and full width at half-maximum of the hydrus V_2O_5 (001) peak using the Scherer equation.²⁷ The results were summarized in Table 1. V_2O_5 films annealed in both nitrogen and air possessed similar interlayer distance of $\sim 11 \text{\AA}$, very close to the interlayer distance of hydrus V_2O_5 with 1.6 water molecules.⁸ However, there was a significant difference in grain size between the samples annealed in nitrogen and air. The grain size of ~ 5.1 nm in the film annealed in nitrogen was about one third of that in the film annealed in air (14.3 nm).

Fig. 2 presents the optical absorption spectra of V_2O_5 films on FTO substrates annealed in air and nitrogen. The inset presents the photo image of the V_2O_5 films after annealing in respective gases. The film annealed in air did not have a color change and remained a yellowish color, but the film annealed in nitrogen turned from yellow to dark green, indicating the presence of V^{4+} and V^{3+} valence states.^{28,29} The shapes of the absorption spectra of the two films were found to be similar, but the absorption band edge of the film annealed in nitrogen was ~ 545 nm, corresponding to a bandgap of ~ 2.28 eV; while ~ 525 nm and ~ 2.37 eV were found for the air annealed film, which agreed well with the reported values between 2.3 and 2.4 eV of V_2O_5 bulk film.^{30,31}

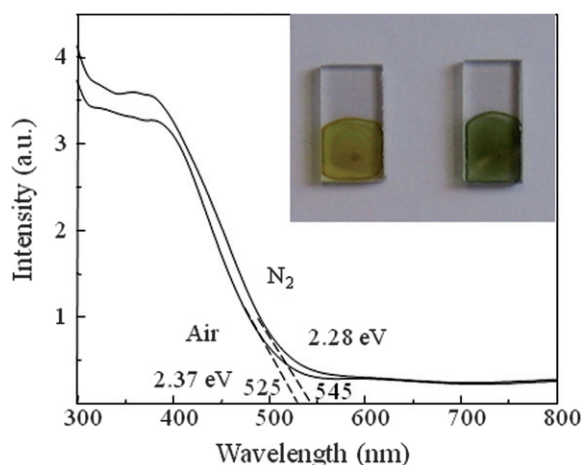


Fig. 2 Absorption spectra of V_2O_5 films annealed in air and nitrogen at $300\text{ }^\circ\text{C}$ for 3 h; the inset presents the photo of films after annealing in air (left) and nitrogen (right) at $300\text{ }^\circ\text{C}$ for 3 h.

The reduced bandgap suggested the presence of extra energy states, probably due to the formation of low valence state vanadium ions such as V^{4+} . It was also reported that V_2O_5 film changed from yellow to green when lithiated, and the absorption edge decreased because of the reduction of partial vanadium ions from V^{5+} to V^{4+} .³² The same or similar change in color and absorption spectra was now found in N_2 annealed film as compared with air annealed one, and suggested that N_2 annealing resulted in partial reduction of V^{5+} to V^{4+} . We are planning to carry out a set of experiments to estimate the ratio of vanadium ions in different valence states. However, the issue is a little more complicated than a simple data point. The ratio of V^{4+}/V^{5+} would decrease with the depth increase from the surface. X-Ray photoelectron spectroscopy (XPS) could tell the accumulated ratio of V^{4+}/V^{5+} of a certain depth region like from the surface to 10 nm into the film. However, it could not tell the ratio of a more in-depth region. We are working on getting a good understanding of the amount of tetravalent vanadium ions and the depth distribution on the electrochemical properties.

The electrochemical impedance spectra (EIS) of the films annealed in air and nitrogen are presented in Fig. 3. Fig. 3a shows the Nyquist plots with the experimental curves as dashed lines and fitting curves as the solid lines; the inset shows the expanded plots at a high frequency region. Fig. 3b shows the equivalent circuit that was used to fit the EIS data. In this circuit, R_1 represents the resistance of the electrolyte; R_2 is the resistance of V_2O_5 film (or the electrode); R_3 represents the charge transfer resistance of the film/electrolyte interface while CPE in the circuit are constant phase elements which are equivalent electrical circuit components that model the behavior of an imperfect capacitor.³³ The parameters estimated through curve fitting were summarized in Table 2. The electrode resistance and charge transfer resistance of V_2O_5 film annealed in N_2 were found to be two thirds of those of the film annealed in air. More specifically, R_2 reduced from $\sim 166\text{ k}\Omega$ in V_2O_5 film annealed in air to $\sim 114\text{ k}\Omega$ in sample annealed in nitrogen, and R_3 decreased from $125\text{ }\Omega$ to $86\text{ }\Omega$. The electrodes measured here were purely vanadium oxides without any conductive additives, so the electrode resistances were much higher than coin-type half cell which was

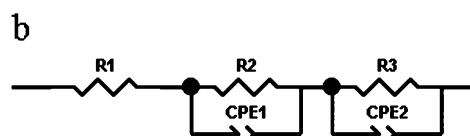
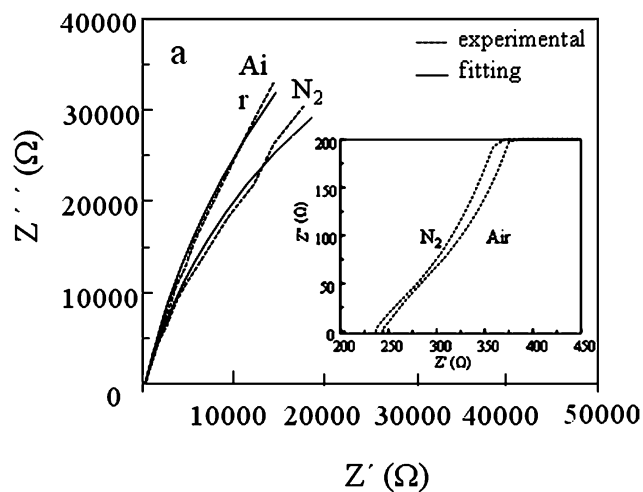


Fig. 3 (a) AC impedance spectra presented as Nyquist plots of V_2O_5 films annealed in air and nitrogen at $300\text{ }^\circ\text{C}$ for 3 h and measured in 1 M $LiClO_4$ in propylene carbonate with testing frequencies from 100 kHz to 0.05 Hz (the inset showing the expanded plots at high frequency region) and (b) the equivalent circuit used to fit the EIS data.

assembled by adding $\sim 10\%$ conductive carbon. The much improved electrical conductivity could be attributed to the formation of V^{4+} and V^{3+} species and possibly also to the associated oxygen vacancies in the film annealed in nitrogen. Similar improvement of electrical conductivity was also found for anodized TiO_2 nanotube arrays after annealing in N_2 .³⁴

The lithium ion intercalation properties of V_2O_5 films annealed in air and nitrogen were studied by means of both cyclic voltammetry and chronopotentiometry. Fig. 4 depicts the initial, twentieth and fiftieth cycle voltammograms of air and nitrogen annealed films tested under the identical conditions with a scan rate of 10 mV s^{-1} . For voltammograms of air annealed film, in the initial cycle, two pairs of noticeable cathodic and anodic peaks were identified with the cathodic peaks centered at -0.12 V and -0.71 V and anodic ones centered at 0.11 V and -0.41 V . There were also two pairs of less distinct peaks with cathodic peaks centered at -0.32 V and -1.24 V and anodic ones centered at -0.17 V and -0.87 V . After 20 cycles, the well defined peaks all became much less intense but did not show obvious position

Table 2 Impedance resistance components for V_2O_5 film electrodes annealed at $300\text{ }^\circ\text{C}$ for 3 h in air and nitrogen environment determined by fitting EIS experimental data measured in 1 M $LiClO_4$ in propylene carbonate using the equivalent circuit shown in Fig. 3b^a

| Electrode | R_1 (Ω) | R_2 (Ω) | R_3 (Ω) |
|--------------------|--------------------|--------------------|--------------------|
| V_2O_5 (Air) | 244 | 166 150 | 125 |
| V_2O_5 (N_2) | 237 | 113 540 | 86 |

^a R_1 = electrolyte resistance; R_2 = electrode resistance; R_3 = charge transfer resistance.

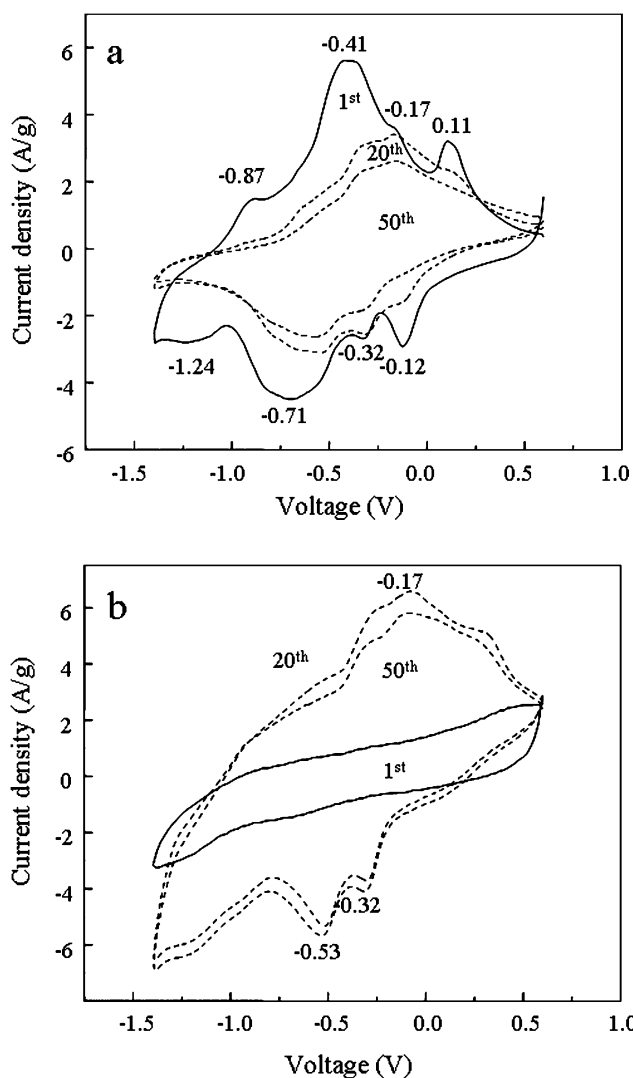


Fig. 4 Cyclic voltammetry curves in the first, twentieth and fiftieth cycles of V_2O_5 films annealed in (a) air and (b) N_2 at $300\text{ }^\circ\text{C}$ for 3 h and measured in 1 M $LiClO_4$ in propylene carbonate with a scan rate of 10 mV s^{-1} in a voltage range between 0.6 V and $-1.4\text{ V vs. Ag/AgCl}$ reference electrode.

shift except the cathodic peak originally centered at -0.71 V shifting to -0.51 V . The originally poorly-defined cathodic peak at -0.32 V and anodic peak at -0.17 V became the most discernible peaks in this cycle. In addition, the sweeping area also decreased noticeably. At the 50th cycle, the curve shape did not change much and peak positions did not shift from those in the 20th cycle, but the sweeping area decreased further. For nitrogen annealed film, no anodic or cathodic peaks were discerned in the initial CV curve and the sweeping area was much smaller than that of the air annealed film. However, after 20 cycles, two cathodic peaks at -0.32 V and -0.53 V and one anodic peak at -0.17 V were discerned, the positions agreeing well with those of the air annealed sample in 20th cycle. In addition, the sweeping area was much larger than that of the initial cycle. From 20th cycle to 50th cycle, the peak positions did not show a noticeable shift and the sweeping area decreased a little, suggesting the good stability of the N_2 annealed film in long term cycles. The

abnormal change of the CV curve shape of N_2 annealed film could be attributed to the surface defects and will be discussed further later in the paper.

Fig. 5 depicts the initial, twentieth and fiftieth chronopotentiometric curves of air and nitrogen annealed films with a charge/discharge current density of 600 mA g^{-1} . There was a noticeable difference in the CP curves for air and nitrogen annealed films. For the air annealed film, the open circuit voltage was $\sim 0.03\text{ V vs. Ag/AgCl}$ reference electrode and the initial discharge CP curve consisted of one plateau from -0.3 V to -0.5 V , about 60 mA h g^{-1} of the total 152 mA h g^{-1} was delivered in this region. The corresponding charge capacity was 130 mA h g^{-1} , 22 mA h g^{-1} lower than the discharge capacity. At the 20th cycle, the shape of discharge and charge curves did not change much but the capacities decreased obviously to 74 mA h g^{-1} and 64 mA h g^{-1} . At the 50th cycle, the capacities decreased further to 44 mA h g^{-1} and 40 mA h g^{-1} . For the N_2 annealed film, the open circuit voltage was $\sim -0.2\text{ V vs. Ag/AgCl}$ reference electrode and the initial discharge and charge curves exhibited

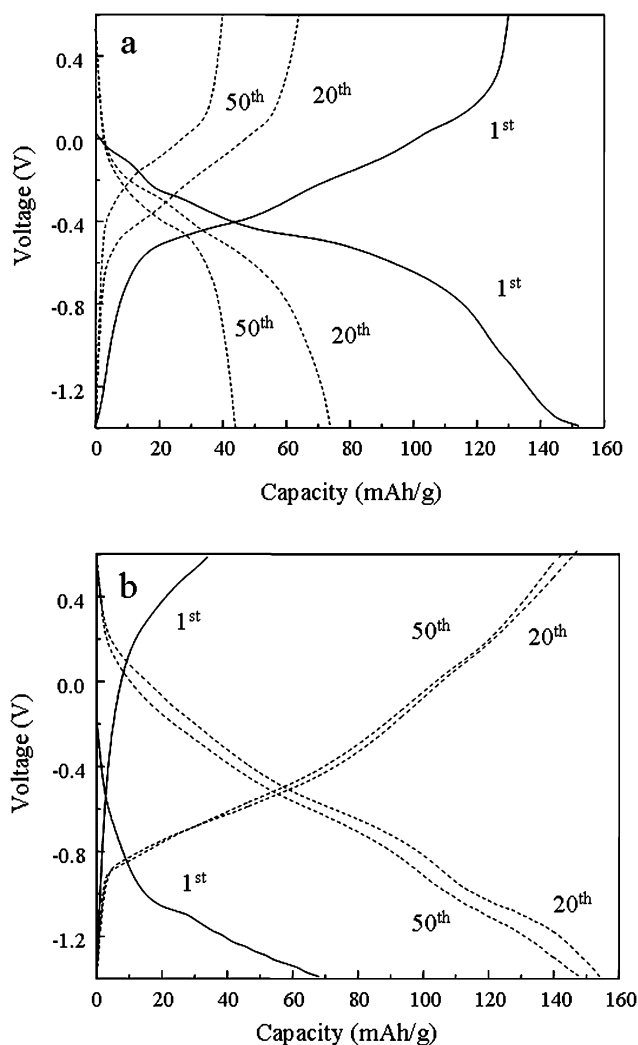


Fig. 5 Chronopotentiometric discharge/charge curves in the first, twentieth and fiftieth cycles at a current density 600 mA g^{-1} of V_2O_5 films annealed in (a) air and (b) nitrogen at $300\text{ }^\circ\text{C}$ for 3 h. Voltage window was 0.6 V to $-1.4\text{ V vs. Ag/AgCl}$ as the reference electrode.

a sloping manner with low capacity values of 68 mA h g^{-1} and 34 mA h g^{-1} . At the 20th cycle, the discharge curve still exhibited a slope decrease, without any detectable lithium ion intercalation plateau as observed in the air annealed sample. While the initial lithium ion intercalation capacity was relatively low, $\sim 70 \text{ mA h g}^{-1}$ at the 1st cycle, it rapidly increased to a high value of 154 mA h g^{-1} at the 20th cycle. The charge capacity also increased from 34 mA h g^{-1} to 148 mA h g^{-1} . At the 50th cycle, the discharge capacity decreased a little to 148 mA h g^{-1} and the charge capacity decreased to 142 mA h g^{-1} . The change in lithium ion intercalation capacity in the nitrogen annealed sample was phenomenal, and the intercalation properties of samples annealed in air and nitrogen differed significantly. The phase transformation associated with the lithium ion intercalation/de-intercalation process in air annealed film was found to be less reversible as evidenced by the relatively larger irreversible capacity in the initial cycle (Fig. 5a) and by the rapid capacity decrease from the initial relatively high value in the 1st cycle to less than 50% in the 20th cycle, and then further to <30% in the 50th cycle. However, the phase transformation process in the N_2 annealed film was found to be very different (Fig. 5b) from that of the air annealed sample. The initial discharge capacity of nitrogen annealed V_2O_5 was relatively low, $\sim 68 \text{ mA h g}^{-1}$; however, the capacity increased sharply and steadily with an increased number of lithium ion intercalation and de-intercalation and reached a high stable value of 154 mA h g^{-1} at the 20th cycle, also with a very low irreversible capacity of only 6 mA h g^{-1} in this cycle. There was a little decrease in the lithium ion intercalation capacity with a further increased number of cycles, which remained as high as 148 mA h g^{-1} even after 50th cycle.

Fig. 6 compares the long term cyclic stability of the air and nitrogen annealed films for lithium ion intercalation measured with a current density of 600 mA g^{-1} for 50 continuous discharge/charge cycles. The poor cyclic stability of air annealed V_2O_5 film is similar to our earlier findings; the relatively larger grain size

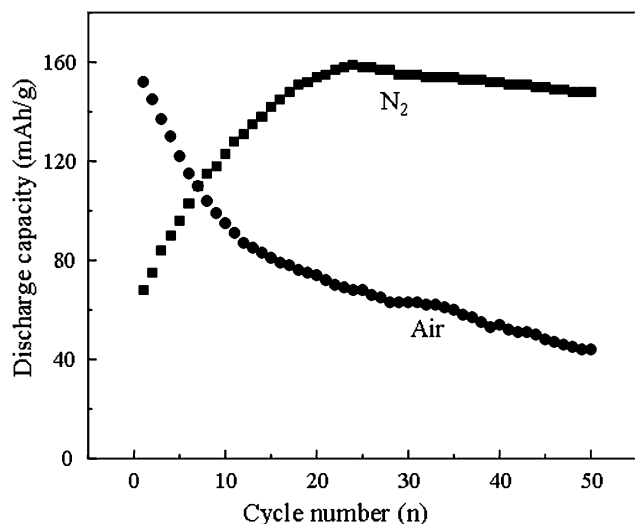


Fig. 6 The Li ion intercalation discharge capacity of V_2O_5 films annealed in air and N_2 at 300°C for 3 h as a function of cyclic numbers. The measurements were carried out in a potential window between 0.6 V and -1.4 V vs. Ag/AgCl as the reference electrode at a current density of 600 mA g^{-1} .

may be responsible.⁸ For N_2 annealed film, mentioned above, before reaching the highest discharge capacity value of 158 mA h g^{-1} at the 24th cycle, it started with a low discharge capacity. While it is not clear what the mechanism is causing such a change in storage capacity with initially low followed by sharp increase with increased lithium ion intercalation and de-intercalation cycles in nitrogen annealed sol-gel derived V_2O_5 film electrodes, the same or similar results or observation have been reported in the literature and some possible mechanisms have been proposed.^{21,35} For example, LiMnO_2 particle electrodes coated with Al_2O_3 and CoO exhibited initial low discharge capacity of 30 mA h g^{-1} but increased quickly in later cycles before reaching a high value of 170 mA h g^{-1} ; it was attributed to the formation of a solid solution at the LiMnO_2 particle and coating interface.³⁵ In later cycles, the coated sample stabilized at the capacity of more than 160 mA h g^{-1} in the reported data of 50 cycles. In contrast, bare LiMnO_2 started with a high discharge capacity of more than 160 mA h g^{-1} but capacity degradation was obvious in later cycles and the discharge capacity was only about 120 mA h g^{-1} after 50 cycles. Our finding is very similar to this reported result. Yet another example is LiFePO_4 electrodes with a poorly crystallized surface layer which was created by annealing in Ar gas. The capacity also exhibited a noticeable increase after an initial cycle and the cyclic stability and rate capability were both improved because of this poorly crystallized surface layer.²¹

The discharge current densities and corresponding intercalation capacities of air and nitrogen annealed films are summarized and compared in Fig. 7. Because of the abnormal capacity increase of the N_2 annealed sample, we used the highest discharge capacity reached instead of the initial discharge capacity. At a relatively low discharge current density, *i.e.* 200 mA g^{-1} , the air annealed sample possessed a little higher discharge capacity of 184 mA h g^{-1} than 178 mA h g^{-1} of N_2 annealed sample. As the current density was increased, both samples exhibited capacity decrease but the N_2 annealed sample had more capacities

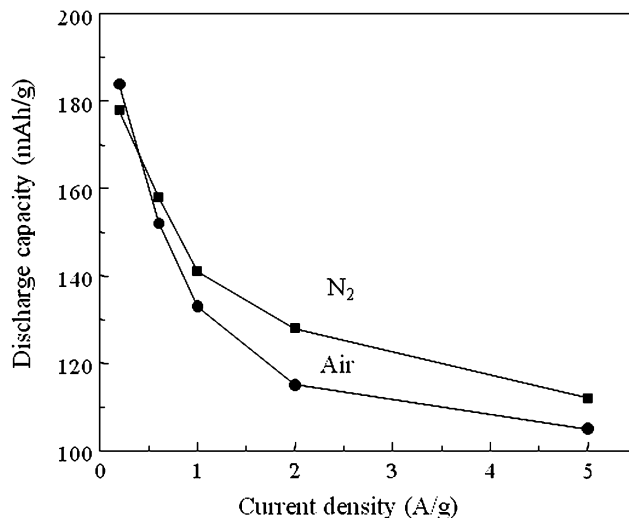


Fig. 7 The discharge capacities of V_2O_5 films annealed in air and N_2 at 300°C for 3 h as a function of applied discharge current densities; for N_2 annealed film, the highest discharge capacity reached in the cycles was used instead of the initial capacity. The measurements were carried out in a potential window between 0.6 V and -1.4 V vs. Ag/AgCl as a reference electrode.

remaining. In detail, the discharge capacities of the N₂ annealed sample were 158 mA h g⁻¹, 145 mA h g⁻¹, 134 mA h g⁻¹ and 122 mA h g⁻¹ corresponding to 600 mA g⁻¹, 1 A g⁻¹, 2 A g⁻¹ and 5 A g⁻¹; while the discharge capacities of air annealed sample were 152 mA h g⁻¹, 138 mA h g⁻¹, 121 mA h g⁻¹ and 105 mA h g⁻¹. The better rate performance of the N₂ annealed sample could be attributed to the improved charge transfer conductivity as found in the impedance measurement which facilitated the interface lithium ion reactions.

The mechanism is not clear why nitrogen annealed vanadium oxide film possessed such different lithium intercalation properties from those of air annealed sample. However, the available experimental data and literature information suggested the surface defects and amorphotization/less crystallization^{21,36,37} may play a significant role in the improved lithium ion intercalation capacity and cyclic stability in nitrogen annealed vanadium oxide films. We also found that when the annealing temperature in N₂ was increased to obviously higher values, *e.g.* 400 °C, more crystallization (*e.g.* larger grain size) was observed in the XRD pattern and films exhibited severe cyclic degradation in the lithium ion intercalation test. This disappearance of good cyclic stability as compared with the 300 °C N₂ annealed film could also be due to the more crystallization induced by higher annealing temperature.

Fig. 8 summarizes and compares the XRD patterns of V₂O₅ films annealed in air (Fig. 8a) and nitrogen (Fig. 8b) before and after 20 cycles and 50 cycles of lithium ion intercalation/de-intercalation. The intensities of the hydrous (001) peak and orthorhombic (001) peak in both vanadium oxide films exhibited a decrease during cycling, suggesting that the crystalline structure of the films got more disordered during cycling.⁷ While the vanadium oxide film annealed in air exhibited little change in the presence and position of XRD peaks in the virgin sample and after 20 or 50 cycles, noticeable differences existed in the XRD patterns of films annealed in nitrogen. Before lithium ion intercalation, there existed two phases: hydrous and orthorhombic vanadium oxides, similar to the sample annealed in air, though with much smaller grain size. After 20 cycles, the intensity of XRD peak corresponding to the (001) peak of orthorhombic vanadium oxide reduced much more appreciably as compared with that of the (001) peak of hydrous vanadium oxide, and totally disappeared after 50 cycles. This suggests that orthorhombic vanadium oxide experienced deterioration in its crystallinity during the lithium ion intercalation, and gradually lost its crystallinity with increased cycles of lithium ion intercalation and de-intercalation. It has been well documented in the literature that poor crystallinity and small grain size favors lithium ion intercalation capacity and cyclic stability.^{8,9,38}

Deteriorating crystallinity might not be the only factor causing such an improvement of intercalation capacity and cyclic stability. The presence of surface defects could contribute significantly to the stability improvement which could be analyzed in three aspects: (1) the interfacial charge transfer ability of the N₂ annealed V₂O₅ film was improved because of the presence of more conductive surface defect species. As has been found out in the optical absorption and impedance analysis, both the optical and electrical conductivity of the film annealed in N₂ was improved compared with film annealed in air due to the presence of V⁴⁺, V³⁺ ions and associated oxygen vacancies on the

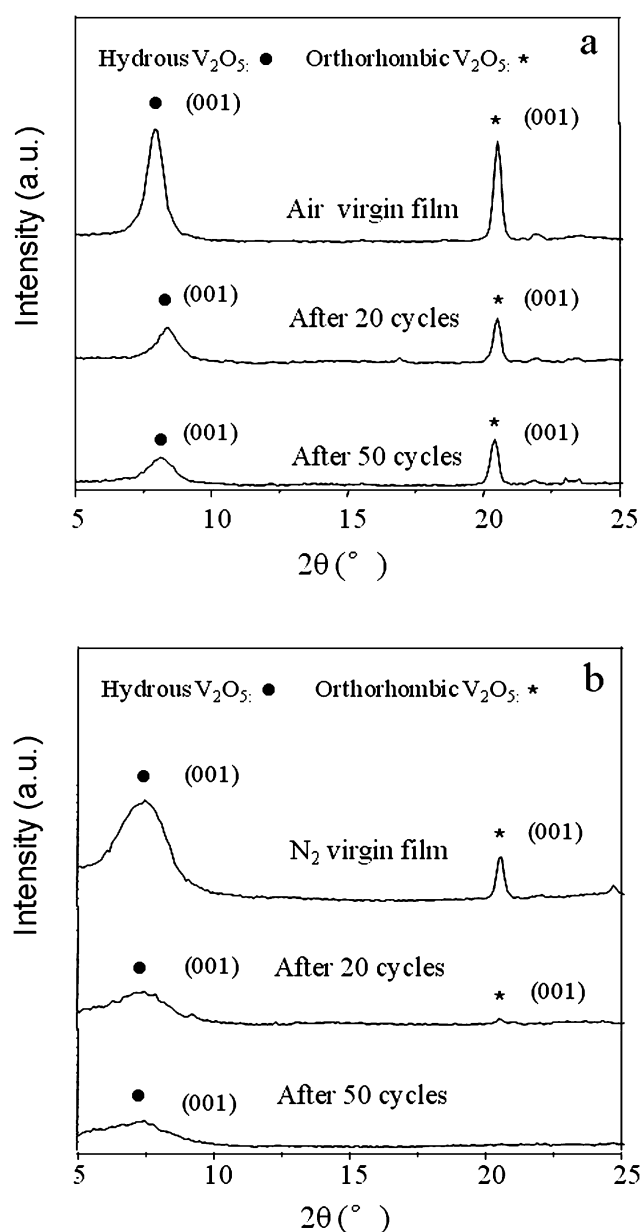


Fig. 8 X-Ray diffraction patterns of V₂O₅ films annealed in (a) air and (b) nitrogen before and after 20 and 50 cycles of lithium ion intercalation and de-intercalation measurements.

film surface. It was found that the intercalation capability of lithium ions into a V₂O₅ xerogel film annealed at high temperature was mainly determined by the interfacial reactions at the electrolyte/electrode interface rather than the lithium ion transport in the bulk oxide electrode.³⁹ Since the enhanced charge transfer conductivity facilitated electron transportation during lithium ion intercalation/de-intercalation at the electrolyte/electrode interface which would obviously facilitate the lithium ion intercalation process,¹⁷ the cyclic stability and rate capability improvement could be justified. Similar improvement after N₂ annealing was also observed in TiO₂ nanotube arrays;⁴⁰ (2) in addition to the conductivity enhancement contribution, the defect layer, like coating layers, also prevented the possible dissolution of V₂O₅ film in the electrolyte and ensured the

integrity of film surface morphology as cycles went on.⁴¹ One of the major causes of lithium ion intercalation capacity degradation in long term cycles was the dissolution of the active material (electrode) in the electrolyte. Building up a protecting layer on the surface will effectively reduce the possibility of electrode dissolution, thus improving the cyclic stability; (3) more than just a simple protecting layer, these surface defects of lower vanadium valence group and oxygen vacancies could also serve as nucleation centers in the phase transformation process that occurred during lithium ions intercalation/de-intercalation.⁴² For this reason, the phase transformation process in the N₂ annealed film was much easier and more reversible just as suggested by the CP curves which exhibited low irreversible capacity (Fig. 5b). The crystal structure was also more stable and the stability of lithium ion intercalation capacities was better than air annealed V₂O₅. This is not the first time that the promoting role of surface defects in lithium intercalation/de-intercalation process has been reported for V₂O₅: V₂O₅ nanorolls with surface cracks exhibited higher capacity than a well-ordered nanoroll structure⁴³ and appropriate defected structure also enhanced the lithium ion intercalation capacity of polycrystalline V₂O₅ film.⁴⁴

4. Conclusions

V₂O₅ film annealed at 300 °C under N₂ gas flow atmosphere exhibited less crystallized phase, enhanced optical absorption and electrical conductivity as compared with film annealed in air under otherwise identical conditions. N₂ annealed vanadium oxide films demonstrated much improved lithium ion intercalation capacity and cyclic stability. Despite that the initial discharge capacity was only 68 mA h g⁻¹ due to the surface defects layer, after 24 cycles, the discharge capacity was as high as 158 mA h g⁻¹. After 50 cycles, the discharge capacity was still 148 mA h g⁻¹. The much improved lithium ion intercalation capacity and cyclic stability could be attributed to the less crystallized structure, the presence of a surface defects layer which not only enhanced the charge transfer conductivity but also behaved like a protective coating layer to ensure the morphology stability of the V₂O₅ film and served as possible nucleation centers to facilitate the phase transformation process during the lithium ion intercalation/de-intercalation process.

Acknowledgements

This work was supported in part by National Science Foundation (DMI-0455994 and DMR-0605159), Air Force Office of Scientific Research (AFOSR-MURI, FA9550-06-1-0326) and Pohang University of Science and Technology, Korea. D. W. L. would like to acknowledge the graduate fellowship (UIF) from the University of Washington Center for Nanotechnology (CNT). B. B. G. would like to acknowledge the NSF-IGERT fellowship (DGE-0654252). A. Q. P. would like to acknowledge the fellowship from the Chinese Scholarship Council.

References

- 1 M. S. Whittingham, *J. Electrochem. Soc.*, 1976, **123**, 315.
- 2 H. K. Park, W. H. Smryl and M. D. Ward, *J. Electrochem. Soc.*, 1995, **142**, 15.
- 3 M. Baba, N. Kumagai, H. Kobayashi, O. Nakano and K. Nishidate, *Electrochem. Solid-State Lett.*, 1999, **2**, 320.

- 4 http://industrial.panasonic.com/www-ctlg/ctlg/qAAA4000_WW.html.
- 5 Y. J. Park, K. S. Ryu, K. M. Kim, N. G. Park, M. G. Kang and S. H. Chang, *Solid State Ionics*, 2002, **154–155**, 229.
- 6 Y. S. Cohen and D. Aurbach, *Electrochem. Commun.*, 2004, **6**, 536.
- 7 Y. Wang and G. Z. Cao, *Electrochim. Acta*, 2006, **51**, 4865.
- 8 Y. Wang, H. M. Shang, T. Chou and G. Z. Cao, *J. Phys. Chem. B*, 2005, **109**, 11361.
- 9 J. X. Wang, C. J. Curtis, D. L. Schulz and J. G. Zhang, *J. Electrochem. Soc.*, 2004, **151**, A1.
- 10 R. Baddour-Hadjean, J. P. Pereira-Ramos, C. Navone and M. Smirnov, *Chem. Mater.*, 2008, **20**, 1916.
- 11 Y. Wang and G. Z. Cao, *Chem. Mater.*, 2006, **18**, 2787.
- 12 S. T. Myung, K. Izumi, S. Komaba, Y. K. Sun, H. Yashiro and N. Kumagai, *Chem. Mater.*, 2005, **17**, 3695.
- 13 D. Li, Y. Kato, K. Kobayakawa, H. Noguchi and Y. Sato, *J. Power Sources*, 2006, **160**, 1342.
- 14 C. Li, H. P. Zhang, L. J. Fu, H. Liu, Y. P. Wu, E. Rahm, R. Holze and H. Q. Wu, *Electrochim. Acta*, 2006, **51**, 3872.
- 15 Y. J. Kim, H. Kim, B. Kim, D. Ahn, J. G. Lee, T. J. Kim, D. Son, J. Cho, Y. W. Kim and B. Kim, *Chem. Mater.*, 2003, **15**, 1505.
- 16 G. T.-K. Fey, Y. Y. Lin and T. P. Kumar, *Surf. Coat. Technol.*, 2005, **191**, 68.
- 17 L. J. Fu, H. Liu, C. Li, Y. P. Wu, E. Rahm, R. Holze and H. Q. Wu, *Solid State Sci.*, 2006, **8**, 113.
- 18 D. W. Liu, Y. H. Zhang, B. B. Garcia and G. Z. Cao, *Electrochim. Acta*, 2009, **54**, 6816.
- 19 Y. H. Zhang, P. Xiao, X. Y. Zhou, D. W. Liu, B. B. Garcia and G. Z. Cao, *J. Mater. Chem.*, 2009, **19**, 948.
- 20 K. Mizushima, P. C. Jones, P. J. Wiseman and J. B. Goodenough, *Mater. Res. Bull.*, 1980, **15**, 783.
- 21 B. Kang and G. Ceder, *Nature*, 2009, **458**, 190.
- 22 S. Pétigny, H. Mostefa-Sba, B. Domenichini, E. Lesniewska, A. Steinbrunn and S. Bourgeois, *Surf. Sci.*, 1998, **410**, 250.
- 23 L. Q. Wang, D. R. Baer and M. H. Engelhard, *Surf. Sci.*, 1994, **320**, 295.
- 24 R. Wang, K. Hashimoto, A. Fujishima, M. Chikuni, E. Kojima, A. Kitamura, M. Shimohigoshi and T. Watanabe, *Nature*, 1997, **388**, 431.
- 25 Q. H. Wu, A. Thissen, W. Jaegermann and M. Liu, *Appl. Surf. Sci.*, 2004, **236**, 473.
- 26 C. J. Fontenot, J. W. Wiench, M. Pruski and G. L. Schrader, *J. Phys. Chem. B*, 2000, **104**, 11622.
- 27 G. Z. Cao, *Nanostructures and Nanomaterials, Synthesis, Properties and Applications*, Imperial College Press, London, 2004.
- 28 D. Zhang, L. B. Su, H. J. Li, X. B. Qian and J. Xu, *J. Cryst. Growth*, 2006, **294**, 437.
- 29 L. C. Klein, *Sol-Gel Optics: Processing and Applications* (The Spring International Series in Engineering and Computer Science) sKluwer Academic Publishers, 1994.
- 30 A. Talledo and C. G. Granqvist, *J. Appl. Phys.*, 1995, **77**, 4655.
- 31 M. Benmoussa, A. Outzourhit, A. Bennouna and E. L. Ameziane, *J. Phys. IV*, 2005, **123**, 41.
- 32 A. Talledo, A. M. Andersson and C. G. Granqvist, *J. Appl. Phys.*, 1991, **69**, 3261.
- 33 P. Xiao, B. B. Garcia, Q. Guo, D. W. Liu and G. Z. Cao, *Electrochem. Commun.*, 2007, **9**, 2441.
- 34 P. Xiao, D. W. Liu, B. B. Garcia, S. Sepehri, Y. H. Zhang and G. Z. Cao, *Sens. Actuators, B*, 2008, **134**, 367.
- 35 J. Cho, T. J. Kim and B. Park, *J. Electrochem. Soc.*, 2002, **149**, A288.
- 36 T. A. Kim, J. H. Kim, M. G. Kim and S. M. Oh, *J. Electrochem. Soc.*, 2003, **150**, A985.
- 37 K. Le Van, H. Groult, A. Mantoux, L. Perrigaud, F. Lantelme, R. Lindstrom, R. Badour-Hadjean, S. Zanna and D. Lincot, *J. Power Sources*, 2006, **160**, 592.
- 38 E. Hosono, T. Kudo, I. Honma, H. Matsuda and H. S. Zhou, *Nano Lett.*, 2009, **9**, 1045.
- 39 S. Pyun and J. S. Bae, *J. Power Sources*, 1997, **68**, 669.
- 40 D. W. Liu, P. Xiao, Y. H. Zhang, B. B. Garcia, Q. F. Zhang, Q. Guo, R. Champion and G. Z. Cao, *J. Phys. Chem. C*, 2008, **112**, 11175.
- 41 Y. Wang and G. Z. Cao, *Adv. Mater.*, 2008, **20**, 2251.
- 42 H. S. Jung, H. Shin, J. R. Kim, J. Y. Kim, K. S. Hong and J. K. Lee, *Langmuir*, 2004, **20**, 11732.
- 43 D. Sun, C. W. Kwon, G. Baure, E. Richman, J. MacLean, B. Dunn and S. H. Tolbert, *Adv. Funct. Mater.*, 2004, **14**, 1197.
- 44 K. E. Swider-Lyons, C. T. Love and D. R. Rolison, *Solid State Ionics*, 2002, **152–153**, 99.